

Conception of a High Resolution X-Ray Computed Tomography Device; Application To Damage Initiation Imaging Inside Materials

E. Cendre ^a, P. Duvauchelle ^a, G. Peix ^a, J.-Y. Buffière ^b, D. Babot ^a

a-INSA-Lyon, CNDRI Bât 303, 69621 Villeurbanne Cedex, France ; peix@insa.insa-lyon.fr

b-INSA-Lyon, GEMPPM Bât 303, 69621 Villeurbanne Cedex, France ; buffiere@gprhp.insa-lyon.fr

Abstract - X-ray computed tomography (CT) offers an unique opportunity for three-dimensionnal (3D) imaging inside most materials (metallic or macromolecular). A non destructive and very quantitative characterization can thus be attained. A 3D tomograph was conceived and constructed, allowing an adjustable spatial resolution with a cubic voxel, which size ranges from 8 to 200 μm . The tomograph is mainly constituted by a microfocus X-ray tube and an X-ray sensitive imager. The small size of the X-ray tube focus (around 7 μm) allows a geometrical enlargement up to 30. Two different imagers can be used : i) an image intensifier (Im.Int.) equipped with a CsI fluorescent screen and a Vidicon camera, ii) a low noise CCD camera (Charge-Coupled Device), equipped with a high-aperture lens and catching the visible image emitted by a terbium-doped gadolinium oxysulfide ($\text{Gd}_2\text{O}_2\text{S}$ [Tb]) fluorescent screen. A mechanical testing machine was constructed that can be set on the turntable, in such a way to image damage initiation along successive states of strain, without dismantling the sample. A stress gauge and a linear displacement sensor allow to record the stress-strain curve. The machine can apply either a tensile or a compressive stress.

Keywords : X-ray, tomography, simulation, low noise camera.

1. INTRODUCTION

The need for non-destructive 3D imaging methods is apparent in many domains : medical diagnostics, biology, earth science, solid state and materials. X-ray tomography has now matured. The start was given in the 1970's by Hounsfield's invention of the first CT scanner. Dedicated to medical imaging, this device brought a Nobel prize (1979) to its inventor. Industrial tomography strongly developed in the 1980's. Our laboratory being mainly concerned by materials characterization, two different tomographs were constructed. The first one, allowing a resolution of 150 μm , has already been described elsewhere [1]. It was mainly dedicated to the characterization of human bone structure, performed "in vitro" on small samples, in connection with mechanical tests. The purpose was to determine the effect of ageing [2] and to establish a structural model able to describe damage initiation inside osteoporotic human bone.

The construction of a second tomograph corresponds to the need for a diversification of our applications : beside biomechanical studies, characterization of composite materials has

proved to be of main importance. The aim is the study of damage mechanisms inside composite materials, whose interest is considerable in the field of transport applications (aeronautic and aerospace). Very precise tomographic images have already been performed using synchrotron radiation [3-4]. In this case, due to the use of phase contrast phenomena, the difference between the matrix and the reinforcement particles appears clearly, even when both materials are nearly similar, from the point of view of their properties of attenuation of X-rays, as it is the case with aluminium and silicon carbide. Nevertheless, as experiments at synchrotron radiation facilities are inevitably scarce, the need for a "laboratory device" was evident, allowing tomography when matrix and reinforcement materials are different, which represents the most general case. The device was projected to offer an adjustable resolution. The possibility to set a mechanical testing machine directly on the turntable, in such a way to image the successive states of damage without dismantling was also of great interest. This tomograph is today available in our laboratory and can be used either with a standard Im. Int. or with a dedicated imaging system whose distinctive features are a

high dynamic range, a large number of pixels (1024x1024), and a high efficiency.

Section 2 will describe the standard Im. Int. used so far, and will give an example of a 3D tomographic image, performed on a human bone sample with a 30 μm resolution, using this device. Section 3 indicates the main characteristics of the microfocus X-ray tube. The dedicated imaging system that was designed and constructed is described within sections 4 (choice of the main features of this system) and 5, (simulation of the characteristics). The time exposure, projected for a set of standard acquisition conditions, is computed, as well as the expected dynamic range. An experimental confirmation of the ability of our imaging system is given. Conclusions are drawn in section 6.

2. DESCRIPTION OF THE IMAGE INTENSIFIER

Im. Int. were developed in the 1950's. Dedicated to medical imaging, they are characterized by a huge amplification, and hence by a very high efficiency, the purpose being to lessen the delivered dose. The Im. Int. used here, equipped with a standard Vidicon-tube camera, is used in front of our microfocus X-ray tube. The pixel size within the delivered image is around 200 μm and the measured spatial resolution is 1.75 line-pair per millimetre (lp/mm) for a Modulation Transfer Function (MTF) of 10% [5]. The 2D images delivered by this device form the individual projections and allow the 3D tomographic reconstruction of the object. Using the possibility of direct enlargement, that is to say setting the sample directly in front of the window of the X-ray tube, allows any spatial resolution between 8 and 200 μm . Figure 1 displays a tomographic image of a human cancellous bone sample. The general features described above were used. A geometrical enlargement of 6.7, which results in a voxel size of 30 μm , was chosen.

As our device is based on the principle of cone-beam X-ray CT, the reconstruction was performed using the generalized fan-beam reconstruction algorithm [6]. We used a programme written by the CEA-LETI, the french organization for nuclear energy applications. This programme offers different kinds of filtration in the frequency domain, and an adjustable voxel size within the reconstructed volume. The reconstructions were effected on a DEC 500 (500 MHz) workstation.

In the field of tomography, Im. Int. is not the most suited imaging device. We will now discuss the reasons why a more specific imaging system was conceived and constructed. The main problems encountered with Im. Int. are the following :

- The very short integration time of the device (40 ms) and the huge amplification generate a strong noise-level. Image summation can be used to increase the signal-to-noise (S/N) ratio, but, due to electronic noise, the overall dynamic range never exceeds some hundreds.

- The images delivered by such a system are distorted in the peripheral part, generating artefacts within the reconstructed volume. For recovering a sound 3D image, a software correction of every projection must be applied.

- The efficiencies of the individual pixels of the Im. Int. are slightly different. During the tomographic acquisition, a given point of the object occupies, within the image, different positions corresponding to different efficiencies. Hence artefacts are generated in the reconstructed volume. A normalization of every projection image can improve the results, but the artefacts are always more or less visible. Moreover, normalization, which implies to divide the current image by a reference image, increases the noise.

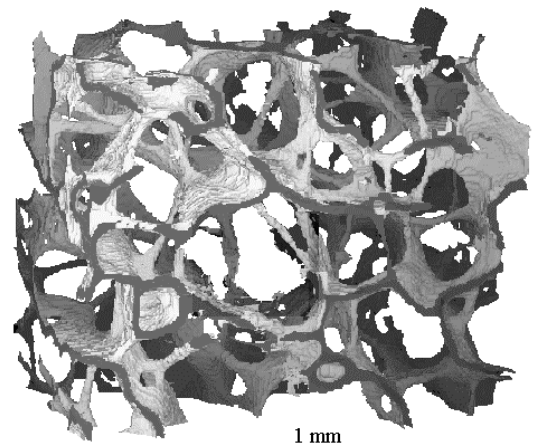


Figure 1: Tomographic image of a human vertebra sample. The use of the Im. Int. with an enlargement of 6.7 resulted in a voxel size of 30 μm .

3. THE X-RAY TUBE

3.1. General features

The HOMX-161 X-ray tube, constructed by the Philips Company, is a microfocus X-ray tube which allows a dissipation of 35 watts with a constant high-voltage, which value is adjustable between 25 and 160 kV. The residual ripple (relative fluctuation of the voltage) is lower than $2 \cdot 10^{-4}$.

3.2. Determination of the focal spot size

The main interest of microfocus X-ray tubes lies in the very low geometrical unsharpness (u_g) generated in the image. A direct enlargement of the image, achieved by bringing the sample close to the focus (and away from the camera) is thus allowed. In fact, the focal spot size of such a device depends on the effective value of the used voltage. Working at 70 kV and taking images of a very thin gold wire with different values of the geometrical enlargement, proved that the resolution is no longer improved for enlargements larger than 30. This limitation corresponds to the fact that u_g becomes greater than the pixel size of the camera. The value of u_g is given by equation (1), which proceeds from a simple geometrical relation :

$$u_g = d(G - 1) \quad (1)$$

In this relation, d stands for the focus size and G for the enlargement ratio. We can therefore estimate the focus size : considering a geometrical unsharpness $u_g = 200 \mu\text{m}$ (which corresponds to the pixel size at the entrance of the Im. Int.), and an enlargement $G = 30$, we found that d was around $7 \mu\text{m}$. As the focus size can be slightly different, depending on the applied voltage, a size in the range $7\text{-}10 \mu\text{m}$ can nevertheless be asserted.

3.3. Fluence rate delivered by the X-ray tube

The main problem, when using a micro-focus X-ray tube, comes from the very low X-ray fluence rate. The first precaution was then to ensure that even the low light emitted by the fluorescent screen was sufficient to deliver, through the lens and CCD, an image with an acceptable dynamic range, and within an exposure time that remains compatible with the acquisition of a whole sinogram. As the number of projections p used for the reconstruction has to respect the general rule [7] :

$$p = \frac{Np}{2} \quad (2)$$

where N stands for the width of the projections (in pixels), it must be pointed out that in the case when projections with a width of 1024 pixels are needed, then approximately 1500 individual projections, regularly spaced all around a 360° rotation of the sample, must be acquired. Therefore, the individual exposure time has to be kept small. The measurement of the real fluence rate emitted by the tube was performed, using an ion-chamber directly set into the X-ray beam.

The next step was to define precisely every component in the imaging system. As the choice of the screen and of the other components (lens and CCD chip) are inter-dependent, a computer

simulation was then performed. Interactions of X-rays within the sample and the fluorescent screen, as well as light emission, were computed. Finally the whole acquisition chain was simulated, leading to a complete adequate solution that will be discussed in the next section.

4. DESIGN OF THE IMAGING SYSTEM

4.1. General features

As shown in Figure 2, a fluorescent screen, set in front of the X-ray tube, delivers an enlarged image of the sample.

This image is caught by a CCD camera and its associated lens ; the mirror allows to set the CCD apart from the main X-ray flux. As the solid angle under which the lens is seen from every point of the screen is low, a high efficiency of the CCD and a high aperture of the lens are needed. This last point requires some attention, as geometrical distortions and spherical aberration must nevertheless remain acceptable. The need for a high dynamic range imposes a reduction of all electronic noises inside the camera, like the readout noise and the noise associated with the dark current. The last one can be kept small by using a cooled CCD chip.

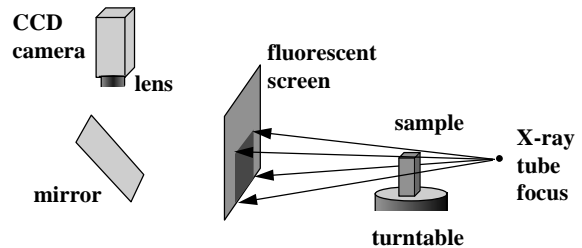


Figure 2 : General scheme of the constructed tomographic system

4.2. Choice of the fluorescent screen

a) thickness of the screen

An increase in the thickness of the fluorescent screen improves its efficiency, absorbing a greater proportion of X-ray photons, but decreases the spatial resolution, because the visible light is scattered inside the fluorescent layer itself.

Figure 3 summarizes two possible experimental conditions.

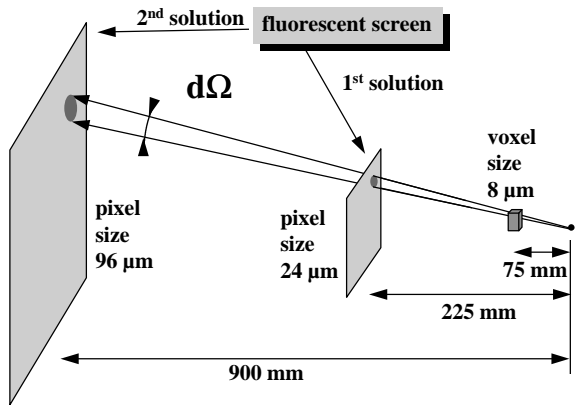


Figure 3 : Scheme displaying the two experimental conditions depicted within the text.

They correspond to respective enlargements of 3 and 12. Considering the case of a voxel size of 8 μm at the level of the sample, which is the highest planned resolution, the corresponding pixel sizes at the fluorescent screen are 24 and 96 μm respectively. The solid angle $d\Omega$ through which every pixel within the screen is seen from the focus is the same in both cases. The corresponding energy brought by the X-ray beam is therefore the same. However the second solution brings two advantages. First, as the scene caught by the camera is larger, the spatial resolution needed is lower and the fluorescent layer can be chosen thicker. The overall efficiency of the imaging system will then be improved. Second, by moving the screen and the camera near the sample, the pixel size can be set at any given value between 8 and 96 μm. Moreover, binning the sensitive elements of the camera inside 2x2 patterns generates images with a resolution extended to 192 μm, to the detriment of the image size (512x512 pixels instead of 1024x1024). The second arrangement was therefore chosen.

The distance of 75 mm indicated between the tube focus and the object corresponds to the size of the mechanical testing machine. When an « in situ » straining of the sample is not necessary, the three distances indicated in Figure 3 will then be reduced by a factor 2, increasing the X-ray flux at the level of the screen by a factor 4.

b) choice of the fluorescent material

The most performant materials which are commonly used are :

- cesium iodide, thallium doped CsI(Tl),
- gadolinium oxysulfide, terbium doped Gd₂ O₂ S (Tb) , often named gadox.

Both materials emit a green light, with a wavelength around 500 nm, and are therefore equivalent, from the point of view of the sensitivity of the CCD chip to the incident light. The main characteristics of both materials are given in table I.

Material	CsI(Tl)	Gd ₂ O ₂ S (Tb)
density (g.cm ⁻³)	4.51	7.50
effective compactness (%)	70	45
conversion yield (%)	10 - 15	5 - 10

Table I : Comparison between the two most performant fluorescent materials

The main difference comes from the physical state of the fluorescent layer. Gadox is available as a powder, with a granular size that can be adjusted between 4 and 24 μm. The powder is mixed with a binding agent and layed out on an aluminium foil. The rule of thumb prescribes a layer thickness of about 85% of the desired spatial resolution which, in our case, implies a thickness in the range 80-85 μm. Cesium iodide is available as very thin needles grown perpendicular to an aluminium foil, through a vapor-deposition process. As the little needles act as a fiber optic plate, preventing light from scattering inside the layer, a thickness equal to 150% of the resolution is generally accepted. It would correspond to a thickness of about 145 μm. Taking into account the thickness of the fluorescent layer and the characteristics of table I, a simulation showed that both screens were equivalent from the point of view of the light yield.

Some problems can be encountered when using CsI, which is slightly hygroscopic and loses its transparency when exposed to wet air. The dry (and transparent) state can however be recovered by warming the screen up to 80° C. We rather selected gadox and ordered for a 80 μm thick layer, which corresponds to a surfacic mass of 30 mg.cm⁻², with a mean granular size of 10 μm. The layer is deposited on a 0.5 mm thick aluminium (Al) foil whose stiffness is sufficient to ensure a good planeity, while attenuation of X-rays remains acceptable (44% of the energy is absorbed by Al when using a voltage of 100 kV). The screen size is dictated by the pixel size at that level, 96 μm for our device, as already mentionned. As CCD chips are square matrix of 1024x1024 square pixels, the size of the screen was set to 100x100 mm.

The above mentionned simulation indicated the number of light photons emitted by the screen. Interpretation of this absolute number and prevision of the dynamic range of the final image is not possible at this stage, because it depends on the light collection by the lens, and on the efficiency and dynamic range of the chip. All these choices being inter-connected, it was necessary to select the CCD chip itself, in such a way to simulate the whole chain.

c) choice of the CCD chip

The results of the simulation proved that the light emitted by the screen was scarce, even for the highest values of the voltage. It was then decided to consider a chip with the best possible efficiency and a very low noise. An "SITe 003 A" charge-coupled device was selected, with a 1024x1024 matrix of square pixels (24 μm x 24 μm). Such a pixel size is among the largest available, most chips offering rather a pixel size of 12 or 19 μm. This characteristic offers the advantage of a better collection of light : the number of electrons that can be stored inside the individual sensitive element of the chip, all along the acquisition, is higher. In the case of the SITe, this number, named the "well capacity", is equal to 300,000 electrons. This is an important feature : for a given electronic noise (like read out noise), a higher value of the well capacity delivers a higher value for the S/N ratio.

The selected chip is also interesting because of the very low value of the "dark current", which corresponds to the summation of electric charges deposited by thermal agitation. This charge is therefore independant of lightening. As the selected chip is of MPP (multi-pinned phase) type, the dark current is very low. It is furthermore reduced when cooling the chip through a triple-stage Peltier cooling device, which can bring the temperature of the chip down to -45 °C, with a stability better than 0.1 °C. Under these conditions, the dark current can be lowered down to 3 electrons per pixel and per second (3 e⁻.pixel⁻¹.s⁻¹). We are now able to compute the noise as a function of the exposure time. For a total exposure of T seconds (exposure time plus read out delay), the number of electric charges gathered in every pixel will then be equal to 3.T e⁻.pixel⁻¹ and, assuming a normal distribution law, the corresponding noise will be (3.T)^{1/2}. This last quantity is estimated in « electron root mean square » (e⁻.rms).

Another important feature to consider is the quantum efficiency (QE) of the chip. This parameter takes into account the capture of light and its conversion into electric charges. The value of QE is extremely high for SITe 003 A : 80% (instead of 30% for most chips). To attain such a high value, the chip is thinned and back-illuminated. For this chip, three offers were considered. In fact, the main differences concerned the camera « controller », the electronic board which monitors the CCD read out. The best offer proposed two possible read out modes :

- a fast-speed mode, used for the preliminary setting of the sample in front of the camera ; the read out time is set to 1 second for the whole frame.

- a low-noise mode, which corresponds to a 5 seconds read out time, preserving a very low read out noise : 10 e⁻ rms.

d) calculation of the lens and optical arrangement

Two possible set up can be considered, as shown on Figure 4. The first one corresponds to the standard situation, encountered in macro-photography. The second uses two lenses. The **collimator lens** is focalized on infinity : the different rays originated from a single point of the screen are sent along parallel directions. The **taking lens**, also focalized on infinity, focuses the image in the CCD plane.

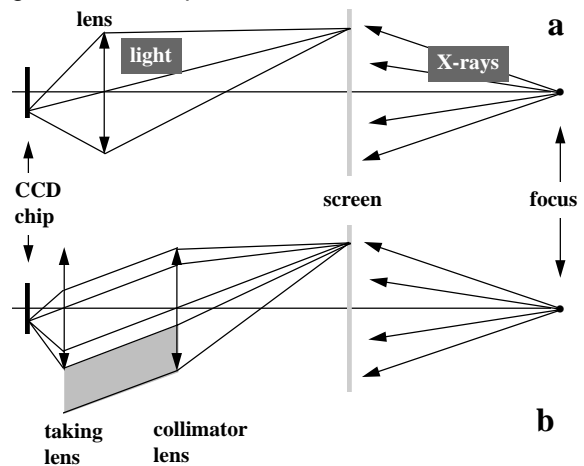


Figure 4 : a) One lens configuration. b) Two lenses configuration : in this case, the vignetting reduces the illumination towards the image edge, in the focal plan of the taking lens. The light drop-off is underlined by the grey area which corresponds to those photons which are lost.

The main advantage of disposal 4b is that both lenses operate when focalized to infinity, which offers a minimum spherical aberration and a maximum focal depth. In the case when the scene to be caught is small (a few centimetres), such a set up delivers a high brightness at the entrance of the camera because the taking lens can be set very near from the fluorescent screen. It is unfortunately prohibited in our case, because of the size of the image to be caught, and therefore of the very high cost of the lens. A problem can arise when both lenses are set too far one from another, because of « vignetting ». This phenomenon, illustrated on Figure 4b, generates a progressive lessening of the luminous intensity towards the edges of the image.

The set up 4a was therefore selected, with two minor fittings intended to lessen the X-ray dose inside the camera :

- a mirror, as already mentioned, was used. It must be noticed that this element was specially ordered for this application : the tin foil must be set on the front side of the mirror, in such a way

to avoid the problem of a phantom image corresponding to that part of light that would be reflected at the entrance in the glass sheet.

- a lead glass, equivalent to 2 mm of lead, was set in front of the lens, in such a way to stop the scattered X-rays and to prevent the ageing of the chip.

The characteristics of the whole imaging system could then be simulated. Figure 5 summarises the whole computation.

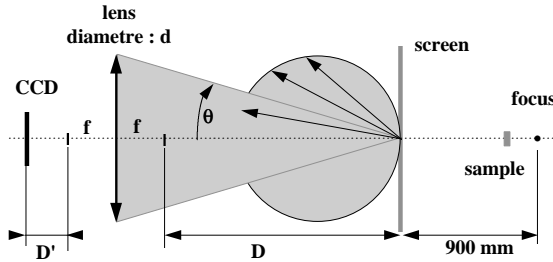


Figure 5 : Computation of the optical system. The lens set in front of the CCD chip is considered here as an unique lens with a focal distance f . The spherical distribution of photons, as shown here, corresponds to the Lambert's law.

A magnification with a ratio γ is obtained when relations 3 and 3' are satisfied :

$$D = \frac{f}{g} \quad \text{and} \quad D' = f \cdot g \quad (3)(3')$$

The number of luminous photons emitted in the whole space by the fluorescent screen (wavelength 500 nm) was computed. We considered, as commonly acknowledged, that an energy of 1 keV (kilo-electron volt) absorbed inside the screen, generates 33.3 luminous photons. Within the hypothesis of a spherical distribution of photons (Lambert's law), as shown on Figure 5, the percentage p of light entering the lens can therefore be computed :

$$p = \sin^2 q \quad (4)$$

and, for a small q angle :

$$p \approx \tan^2 q \quad (5)$$

from geometrical considerations (see Figure 5) we get :

$$\tan q = \frac{d}{2f \left(\frac{1}{g} + 1 \right)} \quad (6)$$

By introducing the ratio f/d which is commonly referred to as « numeric aperture » N , we get :

$$\tan q = \frac{1}{2N} \frac{g}{g+1} \quad (7)$$

and we therefore consider :

$$p = \frac{g^2}{4N^2 (g+1)^2} \quad (8)$$

Taking for N a value of 1.4, which corresponds to an on the shelf lens with a sufficient aperture and a low aberration, and for γ a value of 0.25, which corresponds to the ratio between the pixel size on the screen and on the CCD, we get $p = 0.0051$. Taking into account the efficiency of the lens (0.8) and the transmission throughout the lead glass set in front of the lens (0.7), the total light efficiency of the system is equal to :

$$h_{total} = 2.3 \cdot 10^{-3} \quad (9)$$

5. SIMULATION AND RESULTS

Two different values of the high voltage, 70 and 130 kV, with the respective currents 0.5 and 0.25 mA, and three different areas within the scene were taken into account :

- area A : the X-ray photons reach the fluorescent screen without crossing the sample ; in that case a thickness of 0.5 mm of Al has to be considered, corresponding to the X-ray tube window.
- area B : the X-ray beam passes through a thickness of 2 mm of Al (that is to say 2.5 mm for the overall attenuation).
- area C : the X-ray beam passes through 4.5 mm of Al.

Table II allows the computation of the expected exposure time, that is to say the time that will be necessary to fill the well.

It shows, for both voltages, the number of X-ray photons absorbed in the screen and the corresponding deposited energy, as well as the number of light photons emitted and the number of electrons generated in the well. The exposure time was computed within the conditions of area A, and corresponds to the fact that the final digital image must not be saturated. This value is therefore valid for the whole image, that is to say within the three areas corresponding to the same value of the voltage.

Table II also allows the computation of the dynamic range of the camera. Considering the first case (130 kV), for instance, we find that an exposure time of 19 s with a 5s read out time (which corresponds to 24 s for the whole exposure time) will deliver a dark current of $72 e^-$, (24 times $3 e^-$). The corresponding noise will then be equal to $8.5 e^-$ rms (see section 4.2).

	130 kV			70 kV		
	A	B	C	A	B	C
NA (photons.pixel⁻¹.s⁻¹)	5165	2751	1997	6176	1781	1013
EA (keV.pixel⁻¹.s⁻¹)	2.04 10 ⁵	1.38 10 ⁵	1.09 10 ⁵	1.5 10 ⁵	6.37 10 ⁴	4.1 10 ⁴
NE (photons.pixel⁻¹.s⁻¹)	6.8 10 ⁶	4.6 10 ⁶	3.6 10 ⁶	5.2 10 ⁶	2.1 10 ⁶	1.36 10 ⁶
EI (e⁻.s⁻¹)	15640	10580	8820	11960	4830	3128
T (s)	19			25		
S/N within the X-ray flux	199	153	132	223	150	105
TNA (photons.pixel⁻¹)	98,135	52,269	37,943	154,400	48087	27351
Dark current (e⁻)	72			87		
Electronic noise (e⁻.rms)	13			14		
Total dynamic range	23,076			21,428		

Table II : Computation of the exposure time and of the dynamic range of the camera (simulation). NA number of X-ray photons absorbed in the fluorescent screen ; EA energy absorbed in the fluorescent screen ; NE number of light photons emitted by the screen ; EI number of electrons generated inside the well ; T exposure time to fill the well (300,000 electrons) ; TNA Total number of absorbed X-ray photons (during time T).

Considering besides a read out noise of 10 e⁻ rms and adding both noises in a quadratic way, an overall electronic noise :

$$B = 13 e^{-rms} \quad (10)$$

is obtained. Comparing this value with the highest possible value of the signal (300,000 e⁻ for the full well capacity), the maximum allowed dynamic range is computed. The values thus obtained (23,076 and 21,428) are compatible with the digital numbers supplied at the output of the camera controller, the grey level within the final image being encoded on 14 bits (16384 levels).

An exposure time in the range 20-25 s can then be expected. Taking into account the 5 s corresponding to the read out time, and considering a standard tomographic acquisition, where 900 independant projections are needed, an overall duration of around 6 hours can be projected. It must be considered that those conditions correspond to the worst case : a distance of 900 mm between the X-ray tube and the fluorescent screen corresponds to the highest magnification and delivers a 8 μm resolution at the level of the sample. Setting the device for a 16 μm resolution, a distance of 450 mm can be adopted, reducing the acquisition duration by a factor 4. Furthermore, lessening the distance between the focus and the sample will allow, as already explained, a further reduction of the duration.

The imaging system was constructed according the projected scheme. An Hamamatsu camera was set inside a mechanical assembly similar to Figure 2, and presenting the projected dimensions and characteristics. The CCD chip is set inside the camera under permanent vacuum, which ensures a very simple maintenance. A mechanical shutter completes the camera head. The hot junction of the triple stage Peltier cooling device is thermostated through a chilled water circuit.

The first trials of the imaging system were dedicated to the checking of the overall efficiency : it proved to be slightly better than projected, as the saturation of the camera was attained for an exposure time of 21 seconds with a 70 kV voltage (instead of 25 s).

6. CONCLUSION

Using a simulation software, an X-ray CT device with a high dynamic range (around 20,000) was designed and constructed. All the projected characteristics were attained. Tomographic images are on the point to be performed, but the whole imaging system has already proved to be more convenient than the traditional Im. Int. that was used so far. A large number of applications are now being considered, ranging from medical imaging to advanced materials characterization.

ACKNOWLEDGMENTS

The authors thank the **CEA-LETI** (Grenoble-France) which allowed the free disposition of "eve_recons", tomographic reconstruction software. We particularly acknowledge C. Robert-Coutant and P. Rizo for their help, installing and using eve_recons.

REFERENCES

- [1] V. Kaftandjian, G. Peix, D. Babot, F. Peyrin, "High-resolution X-ray computed tomography using a solid-state linear detector", *Journal of X-ray Science and Technology*, 1996, **6**, pp.94-106
- [2] E. Cendre, D. Mitton, G. Peix, C. Rumelhart, D. Babot, P.-J. Meunier, "Relationship between high resolution X-ray computed tomography measurements and mechanical properties in human lumbar cancellous bone" 12th Int. Bone Densitometry

- Workshop, CRIEFF (U.K.), 18-22 mai 1997, published in *Osteoporosis Int.*, 1997, **7**, (3), p.274.
- [3] J.-Y. Buffière, E. Maire, C. Verdu, P. Cloetens, M. Pateyron, G. Peix, J. Baruchel, "Damage assessment in an Al/SiC composite during monotonic tensile tests using synchrotron X-ray microtomography", *Materials Science and Engineering*, 1997, **A234-A236**, pp.633-635
- [4] P. Cloetens, M. Pateyron-Salomé, J.-Y. Buffière, G. Peix, J. Baruchel, F. Peyrin, M. Schlenker, "Observation of microstructure and damage in materials by phase sensitive radiography and tomography", *J. Appl. Phys.*, 1997, **81** (9), pp. 5878-5886
- [5] Y.M. Zhu, D. Babot, G. Peix, "A quantitative comparison between linear X-ray sensitive array and image-intensifier systems", *NDT International*, 1990, **23** (4), pp.214-220
- [6] L.A. Feldkamp, L.C. Davis, J.W. Kress, "Practical cone-beam algorithm", *J. Opt. Soc. Am*, 1984, **1** (6), pp. 612-619
- [7] C. Kak, M. Slaney, "Principles of Computerized Tomographic Imaging" New York : IEEE Press, 1988